Article

A Mammalian Circadian Clock Model Incorporating Daytime Expression Elements

Craig C. Jolley,[1] Maki Ukai-Tadenuma,[1] Dimitri Perrin,[1] and Hiroki R. Ueda[1,2,3,4,5,*]

[1]Laboratory for Systems Biology, RIKEN Center for Developmental Biology, 2-2-3 Minatojima-minamimachi, Chuo-ku, Kobe, Hyogo 650-0047, Japan; [2]Laboratory for Synthetic Biology, RIKEN Quantitative Biology Center, 2-2-3 Minatojima-minamimachi, Chuo-ku, Kobe, Hyogo 650-0047, Japan; [3]Department of Biological Sciences, Graduate School of Science, Osaka University, 1-1 Machikaneyama, Toyonaka, Osaka 560-0043, Japan; [4]Graduate School of Frontier Biosciences, Osaka University, 1-3 Yamadaoka, Suita, Osaka 565-0871, Japan; and [5]Department of Systems Pharmacology, Graduate School of Medicine, University of Tokyo, Hongo 7-3-1, Bunkyo-ku, Tokyo, 113-0033, Japan

ABSTRACT Models of the mammalian clock have traditionally been based around two feedback loops—the self-repression of *Per*/*Cry* by interfering with activation by BMAL/CLOCK, and the repression of *Bmal*/*Clock* by the REV-ERB proteins. Recent experimental evidence suggests that the D-box, a transcription factor binding site associated with daytime expression, plays a larger role in clock function than has previously been understood. We present a simplified clock model that highlights the role of the D-box and illustrate an approach for finding maximum-entropy ensembles of model parameters, given experimentally imposed constraints. Parameter variability can be mitigated using prior probability distributions derived from genome-wide studies of cellular kinetics. Our model reproduces predictions concerning the dual regulation of *Cry1* by the D-box and Rev-ErbA/ROR response element (RRE) promoter elements and allows for ensemble-based predictions of phase response curves (PRCs). Nonphotic signals such as Neuropeptide Y (NPY) may act by promoting *Cry1* expression, whereas photic signals likely act by stimulating expression from the E/E' box. Ensemble generation with parameter probability restraints reveals more about a model's behavior than a single optimal parameter set.

INTRODUCTION

Systems biology aims to develop predictive mathematical models of cellular phenomena. Models can be abstracted into two components—the model structure, which describes the relationship between modeled quantities and specifies rules for the dynamic updating of these quantities, and the model parameters, which contain problem-specific quantitative information. Although the model structure is often proposed based on expert knowledge of the components of a system and their relationships, identification of model parameters requires quantitative data. Physical scientists prefer models with few parameters, epitomized by von Neumann's famous jibe about fitting an elephant with four parameters (1). Biology involves complex, heterogeneous systems—the components of a cell are far more diverse than are the constituents of a crystal or an atomic nucleus—and quantitative parameter identification is unavoidable.

In what has been termed *sloppy* behavior (2–4), a model's output is strongly affected by certain linear combinations of parameters, whereas other combinations have little impact. When a sloppy model is tuned to agree with system-level data, the uncertainties for the estimates of individual parameters are often disturbingly large. It is only when parameters are viewed in a systemic context that the experimental data show their true (albeit limited) ability to constrain the model.

Given an estimated set of parameters, uncertainty quantification typically involves the calculation of confidence intervals—finite ranges within which the true parameter values can be localized to within a certain probability. In many cases, the confidence interval is infinite and parameters are said to be nonidentifiable. It is often useful to distinguish between practical nonidentifiabilities that result from insufficient or noisy data and structural nonidentifiabilities that arise when there is an insufficient mapping of model states to observables (5).

Confidence intervals can be estimated using the Fisher Information Matrix, which requires linearization about the optimized solution (6). When dealing with highly nonlinear models, it is often preferable to use a bootstrap method, in which parameters are repeatedly reestimated with new experimental data to generate an ensemble of parameter sets (7). Because new data are not always readily available, simulated data can be generated by Monte Carlo techniques, if the variance of the experimental data can be estimated. Bootstrap methods are difficult to apply to models with complex dynamics such as oscillations because parameters often cannot be efficiently reestimated (8). Bootstrap methods allow the estimation of confidence intervals not only for parameters, but also for systems-level outputs of the model.

Submitted January 2, 2014, and accepted for publication July 2, 2014.

*Correspondence: uedah-tky@umin.ac.jp

Editor: Reka Albert

0006-3495/14/09/1462/12 $2.00

http://dx.doi.org/10.1016/j.bpj.2014.07.022

In this study, we use Metropolis Monte Carlo (MMC) sampling (9) to achieve the same goals as bootstrap methods, without the need for repeated reoptimization. The objective function for model optimization was used as an energy function and a maximum-entropy ensemble of parameters with a noise scale similar to the experimental data was generated. This allows us to set bounds on our parameter estimates and model predictions, and determine which of those predictions are robust to changes in the parameter values that are within the experimental noise.

Circadian clocks have long been a fruitful system for mathematical modeling, and the mammalian clock in particular has been the subject of numerous modeling studies (10–14). Most mammalian clock models have focused on two feedback loops. In the first, a CLOCK/BMAL1 heterodimer binds to the E-box region upstream from the *Per* and *Cry* genes, activating their transcription. A PER/CRY heterodimer binds to the CLOCK/BMAL1 complex, abolishing its activity and indirectly repressing the expression of *Per* and *Cry*. In the second loop, the transcription of *Clock* and *Bmal1* are repressed by the binding of REV-ERBα to an RRE region in their promoters, whereas *RevErbα* is controlled by an E-box (and therefore by CLOCK/BMAL1 and PER/CRY). Some researchers (12) have referred to this as a positive feedback loop, emphasizing that *Bmal1* and *Clock* indirectly activate their own transcription by activating *Per* and *Cry*, which repress *RevErbα* and therefore derepress the RRE-controlled *Clock* and *Bmal1* genes. Others (11) have modeled *Bmal1* as self-inhibitory because BMAL1 is also a direct activator of *RevErbα*. *RevErbα*$^{-/-}$ knockout mice show only a modest circadian phenotype, and most modeling studies assume that the loop involving *RevErbα* serves only a stabilizing or regulatory role and that oscillations should persist in its absence. Recently, *RevErbα/β* double knockout mice have been used to show that the (partially redundant) *RevErb* genes are essential; double-knockout mice show phenotypes similar to knockouts of core clock genes such as *Per* and *Bmal1* (15).

Recently, a different organizational scheme has been proposed (Fig. 1 *A*) (16–18). This approach focuses on three clock-controlled elements (CCE), transcription factor (TF) binding sites that give their target gene a circadian expression schedule. These three are the E/E'-box, which governs morning expression (19–22); the D-box, which promotes daytime expression (21,23); and the RRE, which leads to evening expression (21,24–26).

When an exogenous luciferase reporter is competitively regulated by an E/E'-box-driven promoter and an RRE-driven repressor, the result is a daytime expression phase similar to that obtained when the reporter is driven by a D-box. In other words, combining morning activation and nighttime repression generates a D-box. Similarly, a nighttime phase characteristic of RRE expression can be obtained by combining a daytime promoter and a morning repressor

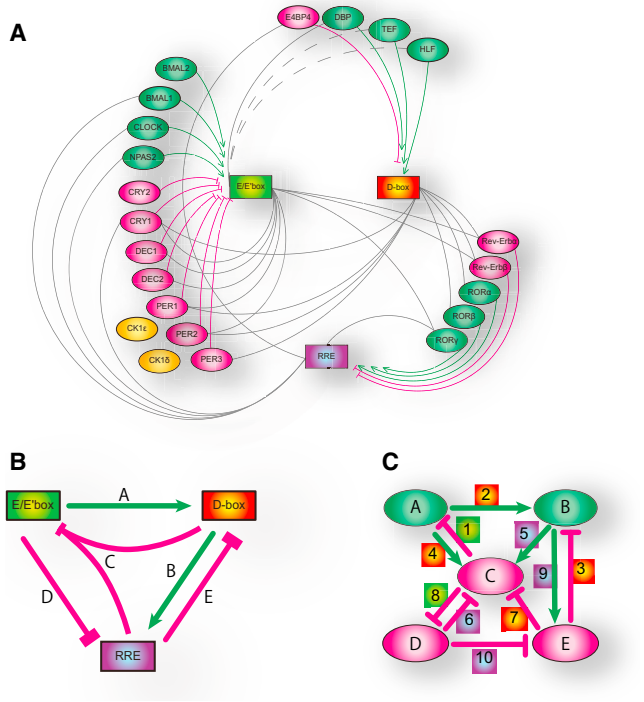

FIGURE 1 (*A*) The core clockwork involves transcriptional activators (*green*), repressors (*magenta*), and protein kinases (*yellow*). Transcriptional regulation involves three clock-controlled elements: the E/E'-box, the D-box, and the RRE. Gray lines indicate that a transcription factor (TF) is regulated by a particular CCE, magenta or green lines indicate the CCE to which a given TF binds. Dotted lines denote computationally inferred relationships. (*B*) Simplified version, motivated by synthetic-biology experiments. (*C*) Realization of the simplified clock architecture using two activators and three repressors. Numbered boxes show regulatory interactions, color-coded by CCE. To see this figure in color, go online.

(17). *Cry1* contains an E/E'-box and D-boxes in its promoter, as well as an RRE in an intron (18). When exogenous *Cry1* was driven by an engineered promoter in cultured *Cry1*$^{-/-}$:*Cry2*$^{-/-}$ cells, a combination of D-box and RRE elements recapitulated the wild-type behavior, whereas the (widely assumed) E/E'-box/RRE combination led to aberrant circadian rhythms. CRY1 is an E/E'-box repressor with an evening expression phase; reconstructing the E/E'-box expression using D-box and RRE elements completes the simplified network shown in Fig. 1 *B* and *C*.

This topology differs from the canonical clock structure in several ways. Instead of a deconstructive approach in which system components are identified and their interactions characterized, it is informed by a synthetic approach in which interactions are added until the desired system behavior can be replicated. As a rule, clock modeling studies have neglected the D-box. Although the essentiality of the D-box is still unclear (27), its role in *Cry1* regulation argues for its importance.

Our study should be placed in the context of previous clock models (10–14). The clearest difference is our inclusion of genes regulated by the D-box; previous studies

have focused primarily on the *Per*, *Cry*, *Bmal*, and *RevErb* genes, with the possible inclusion of *Clock* (11,13,14), *Rorγ* (13), *Npas* (14), and various circadian kinases (14). The model by Mirsky et al. uses *Rorγ* to capture the effects of all of the *Ror* activators; this accounts for the combinatorial regulation of *Rorγ* by the E/E'-box and the RRE, but not the regulation of *Rorα* and *Rorβ* by the D-box (21). Although recent experiments suggest dual regulation of *Cry1* by RRE and D-box elements, previous models have described *Cry1* as regulated either by an E-box alone (11,12) or by an E-box together with an RRE (10,13,14). Although the precise role of the D-box is likely to remain controversial, inclusion in modeling studies should be a part of future assessments of its function.

Another important difference is in computational methodology. Early modeling studies (10–12) used manual, trial-and-error parameter searches. Later studies used global search strategies such as evolutionary optimization (13) or simulated annealing (14); our work follows this more recent trend by using differential evolution (28) for optimization. Previous studies assessed the model's robustness primarily by modifying individual parameters; our method provides a more comprehensive picture of parameter variability by using MMC sampling, and is somewhat in the spirit of clock modeling studies that have used bootstrap sampling (8).

Finally, previous clock models have been validated primarily based on their ability to predict knockout mutants, including some subtle and counterintuitive effects. Doing this successfully often requires the inclusion of multiple isoforms of the *Cry*, *Per*, and *Bmal* genes, to capture their partial functional redundancy (13,14). Our study has focused instead on a minimal model inspired by synthetic-biology approaches; redundant isoforms are omitted and many of the relevant knockouts have not yet been characterized. Instead, we use our model to make predictions regarding the phase response curves obtained by perturbations of different genes, and outline how these phase response predictions might be experimentally accessible.

MATERIALS AND METHODS

Model equations

The gene regulatory network can be represented as a system of ordinary differential equations (ODEs). The mRNA variables a to e and the protein variables A to E correspond to circadian clock genes as listed in Table 1.

TABLE 1 Possible assignments of model genes to mammalian clock genes

Model gene	Mammalian clock gene(s)
a	*Dbp/Tef/Hlf*
b	*Rorα/β*
c	*Cry1*
d	*Rev-Erbα/β*
e	*E4bp4*

$$\begin{aligned}
\frac{da}{d\tau} &= h_1(C) - \eta_{ma}a & \frac{dA}{d\tau} &= a - \eta_{pA}A \\
\frac{db}{d\tau} &= g_{2,3}(A,E) - \eta_{mb}b & \frac{dB}{d\tau} &= b - \eta_{pB}B \\
\frac{dc}{d\tau} &= g_{4,7}(A,E) + g_{5,6}(B,D) - \eta_{mc}c & \frac{dC}{d\tau} &= c - \eta_{pC}C \\
\frac{dd}{d\tau} &= h_8(C) - \eta_{md}d & \frac{dD}{d\tau} &= d - \eta_{pD}D \\
\frac{de}{d\tau} &= g_{9,10}(B,D) - \eta_{me}e & \frac{dE}{d\tau} &= e - \eta_{pE}E
\end{aligned} \tag{1}$$

Details of the model equation derivation can be found in the Supporting Material. The dependent variables a to e and A to E are unitless; the absolute concentration scales are arbitrary and we are only interested in relative changes. The η parameters are unitless degradation rates of mRNAs and proteins. The functions $h(R)$ and $g(A,R)$ are used to capture the effects of gene regulation; both are bounded to the interval [0,1], with $h(R)$ monotonically decreasing (repression), and $g(A,R)$ increasing in A but decreasing in R (activation and repression on the same promoter). Binding follows the Hill equation; activators and repressors bind competitively to the same promoter as in the following:

$$H_i(R) = \frac{1}{1+(\chi_i R)^n} \qquad g_{i,j}(A,R) = \frac{(\chi_i A)^n}{1+(\chi_i A)^n+(\chi_j R)^n} \tag{2}$$

Here, the χ_i's are dimensionless activation constants—low χ_i values correspond either to weak binding or low-abundance TFs. To limit the number of free parameters, the Hill coefficient n was assumed to be equal for all reactions.

If all dimensionless degradation rates (the η's in Eq. 1) are multiplied by a factor γ_t and all of the activation constants χ are multiplied by γ_t^2, then the period will decrease by $1/\gamma_t$, whereas the model output is otherwise unchanged.

Knockout phenotype constraints

The circadian clock is rather resilient against gene knockouts (13,15,27), especially at the organism level, but our simplified model lacks redundancy and is more easily rendered arrhythmic. Rather than modifying Eq. 1, we can obtain knockout effects by setting some of the χ_i variables to zero. For example, a *Dbp/Tef/Hlf* triple knockout could be approximated by setting $\chi_2 = \chi_4 = 0$; levels of the protein variable A will still be nonzero, but it will not have any effect on the other variables. In reality, mice with this triple mutation are rhythmic (albeit prone to epilepsy). The simulated knockout is always arrhythmic, because b and c are always zero in the absence of A, and no closed feedback loops exist. Other knockout phenotypes disturb clock function in ways that significantly constrain our model. The *Cry1/2* (29) and *Rev-Erbα/β* double knockouts (15) show complete arrhythmicity. Fig. 1 *C* shows that the removal of *Cry1* disrupts all feedback loops and makes oscillations impossible.

Removal of *Rev-Erbα/β* leaves some feedback loops intact, and parameter sets with $\chi_6 = \chi_{10} = 0$ are sometimes rhythmic. In another interesting set of mutants, either the D-box or the RRE has been removed from *Cry1* (18); removal of the RRE leads to arrhythmicity, whereas D-box removal lengthens the oscillation period. Correct phenotypes for these mutations are not guaranteed by the model topology.

To ensure correct knockout phenotypes, our model was reintegrated three times: once with $\chi_6 = \chi_{10} = 0$ (*Rev-Erb* knockout), once with $\chi_5 = \chi_6 = 0$ (*Cry1*ΔRRE), and once with $\chi_4 = \chi_7 = 0$ (*Cry1*ΔD-box). If any of these did not produce the correct oscillation phenotype (arrhythmic, arrhythmic, and long-period, respectively), the objective function (see below) was set to ~10^{300} (the maximum double-precision floating point value), effectively removing these parameter sets from consideration.

Parameter search

Initially, parameters were chosen randomly from the probability distributions described in Table S1 and Fig. S1 in the Supporting Material. The distribution of mRNA decay constants was derived from the data set of Sharova et al. (30), who measured the decay rates of 1825 TF mRNAs in a mouse cell culture. The rate distributions for mRNA transcription, as well as protein translation and degradation, were drawn from Schwanhäusser et al. (31), who used parallel metabolic pulse labeling to estimate these rates for more than 5000 genes in mammalian cells. The distribution for TF-DNA binding constants was chosen to have significant density over the range from 0.002 to 10 nM (32), but to have a density near zero for values above 1000 nM, a region dominated by nonspecific binding (33). The nondimensional parameters χ and η above were obtained from these distributions as described in the Supporting Material. The pairs (χ_1, χ_8), (χ_2, χ_4), (χ_3, χ_7), (χ_5, χ_9), and (χ_6, χ_{10}) were constrained to be equal in the initial search, because they describe the binding constants for a single TF on similar promoters. For each randomly chosen parameter set, the fixed point was identified using a multidimensional Newton search (6) and the stability determined from the eigenvalues of the Jacobian $J_{ik}(t) = \partial f_i(t)/\partial y_j$ at the fixed point (34).

In this initial search, ~ 1.86% of parameter sets showed limit-cycle oscillations. When knockout constraints were included in the initial search, the success rate decreased to 0.015%. Because the experimental parameter distributions were measured for a broad range of cellular genes, rather than specifically for oscillating transcription factors, one can expect to see some systematic differences between the distribution used in the search and the distribution of parameters in successful oscillators. Typical oscillation periods were around 200 h; parameters were rescaled as described above to give 24-h periods. In general, this led to degradation rates that were faster in the oscillating parameter sets than for cellular genes and proteins generally. To compensate for this difference, we calculated new parameter distributions from the search results that were used in scoring (Fig. S1).

Estimating protein oscillation phases

Model genes were identified with real circadian genes (see Table 1) for which qPCR data were available for mRNA abundances in the mouse Suprachiasmatic nucleus (SCN) (21). The available protein data were far less quantitative; published results (22,35–38) were available only for proteins sampled from the mouse liver, typically at 4-h time intervals, and (roughly) quantified by Western blotting. Our approach was to estimate amplitudes from published data and use the amplitude data to derive other features of the protein abundance curves.

Protein amplitudes were obtained either by calculating band densities from published blot images using ImageJ (39), or (when band densities were quantified in the original publication) converting published plots into a data table format using Engauge (http://digitizer.sourceforge.net/). For DBP and REV-ERBα, oscillations were so large that a reliable cosine fit was impossible; these were assigned a conservative oscillation amplitude of 0.8. The amplitudes obtained by curve fitting for CRY1 (= 0.521) and E4BP4 (= 0.461) were usable. No oscillation amplitude could be obtained for (ROR)α because, in contrast to the SCN, it does not oscillate in the mouse liver. A conservative value of 0.25 was assigned, equal to the smallest oscillation amplitude found for any circadian protein (CLOCK).

To estimate physically reasonable mRNA-protein phase lags, an mRNA m and a protein p were modeled using the following:

$$\frac{dm}{dt} = \frac{1}{2}\left(\cos\frac{2\pi t}{24} + 1\right)\beta_m - \alpha_m m$$
$$\frac{dp}{dt} = \beta_p m - \alpha_p p \tag{3}$$

These equations can be solved analytically (see Supporting Material) to obtain an asymptotic protein oscillation amplitude of

$$\frac{\alpha_m \alpha_p}{\sqrt{\left(\alpha_p^2 + \omega_0^2\right)\left(\omega_0^2 + \alpha_m^2\right)}}. \tag{4}$$

The phase lag between the mRNA and protein oscillations is obtained using the following:

$$\tan^{-1}\left(\frac{\alpha_p \sin\varphi + \omega_0 \cos\varphi}{\alpha_p \cos\varphi - \omega_0 \sin\varphi}\right) - \varphi \quad \varphi = \tan^{-1}\frac{\omega_0}{\alpha_m} \tag{5}$$

Note that both quantities depend only on the degradation rates α_m and α_p, and the driving frequency $\omega_0 = 2\pi/24$. When values for α_m and α_p were drawn at random from the experimentally derived distributions in Table S1, a roughly linear relationship was found between phase lag and protein amplitude (Fig. S2). This allows us to estimate physically reasonable phase lags based on protein amplitudes. For DBP, CRY1, REV-ERBα, and E4BP4, the resulting phase lags were consistent with the available Western blot data. The higher-amplitude proteins (DBP and REV-ERBα) were assigned the shortest delays (1.7 h) whereas E4BP4 was given a longer delay (3.4 h). For protein RORα, Western blot data was unavailable and the phase lag was set to 4.5 h, consistent with the relatively low amplitude assumed above. These phase lags were then added to the (more accurate) mRNA phases to obtain the target phases depicted in Fig. S3.

Definition of the objective function

Parameter sets were scored by integrating the dynamical equations until they converged to a limit cycle, then measuring the total squared deviation between the experimentally derived data points and the model abundances (Figs. 2, Fig. S4). For the protein components, cosine curves were calculated using the amplitudes and phases described above, with the same sampling density (12 points over 48 h) as the qPCR data. The published qPCR data (and the estimated protein data) had been normalized to have a mean of 1.0. Because the model equations are nondimensional, the absolute oscillation baseline is arbitrary and model outputs were similarly normalized before comparison. The score function should be insensitive to initial conditions, so the score is minimized relative to an arbitrary phase shift φ as in the following:

$$S = \min_{\phi}\left(\sum_{x\in\{a,b,c,d,e,A,B,C,D,E\}}\sum_{i}\left(\exp(x,t_i) - \text{model}(x,t_i+\phi)\right)^2\right) \tag{6}$$

In addition to measuring the quality of the model output, one can assess the plausibility of the model parameters themselves. The previous probability of each individual parameter value p_j was calculated using the probability distributions P_j obtained from the initial parameter search (see Table S2).

$$\Psi = -\ln\left(\prod_j P_j(p_j)\right) + \ln\left(\prod_j \max(P_j)\right) \tag{7}$$

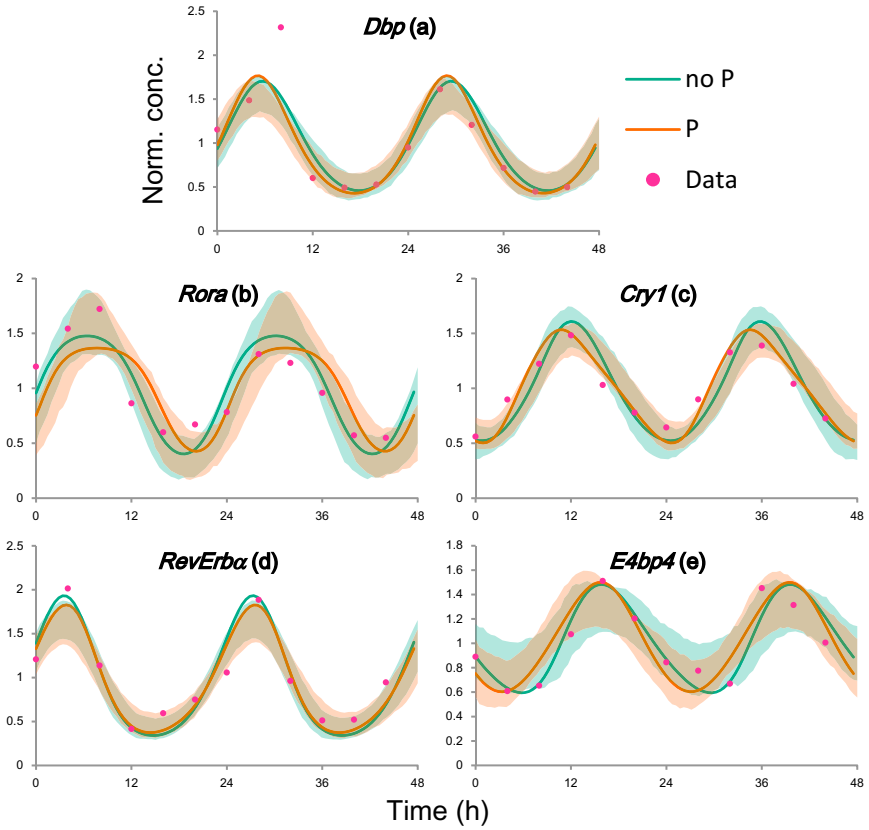

FIGURE 2 Ensemble-based predictions of mRNA levels. Parameters were chosen by minimizing the total squared deviation from the data points shown, either without ("no P") or with ("P") probability constraints on parameter values. Bold lines show the output for the optimized parameter values; shaded areas contain 80% of the traces from Monte Carlo ensembles. Similar plots for the protein components can be found in Fig. S4. To see this figure in color, go online.

In some of the calculations described below, this term was added to the score function defined above.

$$S_P = S + \gamma\Psi \tag{8}$$

The weighting term γ controls the relative balance between the two components. The value chosen (0.1) was sufficient to constrain the distribution of model parameters without severely compromising the quality of the fit (Fig. 2).

Parameter set optimization

Parameters were optimized using a differential evolution (DE) algorithm (28). 10^4 oscillating parameter sets were randomly generated from the distributions in Table S1 and rescaled to have 24-h periods; the 256 highest-scoring sets were used as the starting population. DE converged on a near-optimal parameter set; the result was further refined by simplex minimization (40).

Generation of model ensembles

Once a global optimum was identified, an ensemble of nearby points could be generated using the MMC algorithm (9). The fitted qPCR data comprised five transcripts, sampled every four hours over a 48-h period; an error scale was established by calculating the median absolute deviation between the model results and these 60 data points. An MMC sampling temperature was chosen that gave roughly the same median absolute deviation between the optimized model and the members of the ensemble. The scoring schemes with fewer constraints (i.e., omitting the parameter-probability and knockout terms) were able to fit the experimental data more closely and therefore required lower-temperature MMC sampling to generate an ensemble with the same median error.

Generation of phase response curves

Phase response curves (PRCs) were generated following the method of Kramer et al. (41). Briefly, a general set of coupled ODEs with a parameter vector $\boldsymbol{\alpha}$ can be written as in the following:

$$\frac{dy}{dt} = \mathbf{f}(\mathbf{y}, \boldsymbol{\alpha}, t) \tag{9}$$

We consider $\boldsymbol{\alpha}$ to include not only the parameters that enter explicitly into $\mathbf{f}$ but also the initial conditions $\mathbf{y}(0)$. Using the Jacobian, we can calculate the adjoint Green's function matrix as in the following:

$$\frac{d}{dt'}\mathbf{K}^{\dagger}(t',t) + \mathbf{K}^{\dagger}(t',t)\mathbf{J}(t') = \mathbf{0}, \quad \mathbf{K}^{\dagger}(t,t) = \mathbf{I}, \; t' \le t \tag{10}$$

Once the system has converged to the limit cycle, its state can be completely described by specifying its phase along the limit cycle trajectory. A differential perturbation ∂y_k to the state variable y_k, delivered at time t', will lead to a differential delay or advance ∂t that can be calculated as in the following:

$$Q_k(t') = \frac{\partial t}{\partial y_k(t')} = \lim_{t\to\infty} -K^{\dagger}_{jk}(t',t) \Big/ \frac{dy_j(t)}{dt} \tag{11}$$

In practice, this calculation requires integrating Eq. 9 (in our case, Eq. 1) forward from a defined starting point on the limit cycle to time t and saving values of $\mathbf{J}$ at all of the integration time points. The $t\to\infty$ limit is satisfied as long as the forward integration has adequately converged to the limit cycle. $\mathbf{J}$ must then be interpolated (e.g., using a cubic spline) to give values at arbitrary time points for the integration of Eq. 9 backward to time t'. This backward integration only needs to be performed once; one can save the

values of **K** at each integration time point and interpolate between them to obtain $Q_k(t')$ at arbitrary times.

It is also possible (albeit less precise) to calculate PRCs by a method resembling an experimental protocol, in which state variables or model parameters are perturbed at a defined point during the integration and the resulting phase shift measured. This method produces curves with different magnitudes, but roughly the same shapes.

RESULTS

Ensemble parameter distributions

Fig. 3 shows the distribution of parameters obtained under four different scoring conditions: both with and without the probability constraints ("P") and the knockout constraints ("KO"). For each set of conditions, 6400 parameter sets were sampled from the MMC ensemble and the pooled set of 25,600 parameter sets, along with the four optimized solutions, was projected onto their first two principal components and visualized using minimum-area convex hulls (Fig. 3 *A*). The ensembles with probability constraints occupy a smaller area than those without them, illustrating

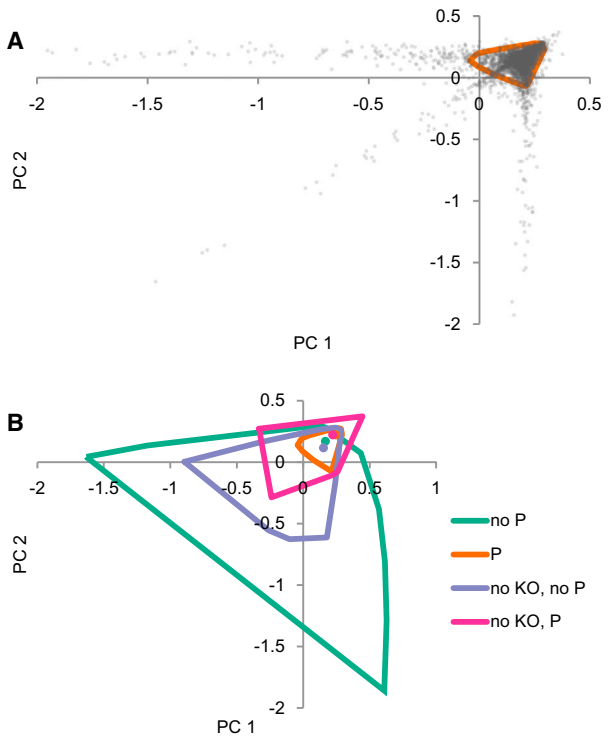

FIGURE 3 (*A*) Parameter values were drawn from a Monte Carlo ensemble and projected onto their first two principal coordinates. The solid lines show a minimum-area convex hull containing 90% of points. (*B*) Minimum-area convex hulls for parameter sets sampled under four different scoring conditions: both with and without the parameter value probability constraints ("P" versus "no P") and either with or without ("no KO") the knockout constraints. Locations of optima are shown by round dots. The probability constraint generally results in a smaller sampling region, and removal of the knockout constraints permits the exploration of otherwise forbidden regions of parameter space. To see this figure in color, go online.

the constraints' success in limiting access to unrealistic parameter values. The calculation with neither probability nor knockout constraints ("no KO, no P") occupies a smaller area than the version with knockout constraints only ("no P"); this is likely because the "no KO, no P" calculation could provide a closer fit to the experimental data and was therefore sampled at a lower temperature. The "no KO" sampling also ventures into regions of parameter space that appear to be inaccessible when the knockout constraints are present. Fig. S5 shows the degree to which knockout constraints are violated when they are not enforced during optimization and sampling. When the probability constraints are present but the knockout constraints are not ("no KO, P" in Fig. 3 *B*), the arrhythmic *RevErb* knockout phenotype is almost never reproduced correctly. This appears to result from specific changes in the parameter distribution.

Fig. 4 presents another perspective on parameter variability—here individual parameter values are compared across the same four sampling schemes. Again, the two ensembles using the probability constraint show less variation in parameter values than the two that omitted it.

One unanticipated effect of the probability constraint term is that strong regulatory interactions (i.e., large χ values) were compensated by weakening other interactions, often to the point of insignificance. The net effect was a "pruning" of the regulatory network that identified interactions that may not be important for the correct functioning of the model. For example, χ_3 and χ_7, the parameters controlling E4BP4's interactions with *Rorα* and *Cry1*, were lower than the other χ parameters. When these were set to zero (i.e., an *E4bp4* knockout), rhythmicity was nearly always retained. This suggests that *E4bp4* may function primarily as a circadian output gene, rather than as a member of the core clock network. Similar effects are observed for χ_9 and χ_{10}, the parameters controlling the regulation of *E4bp4*.

Similar pruning effects allow us to clearly see the effects of knockout constraints. The clearest effect of the knockout constraint (i.e., the difference between "P" and "no KO, P") is in the values of χ_4 and χ_6, the parameters that control regulation of *Cry1* by DBP (via the D-box) and REV-ERBα (via the RRE), both of which are repressed by CRY1 via the E/E'-box. Fig. S5 suggests that the major difference between these two ensembles is that the knockout-unconstrained ensemble fails to reproduce the *RevErb* knockout phenotype. In other words, a correct *RevErb* knockout phenotype is correlated with the regulation of *Cry1* by E/E'-box-controlled genes. If other clock genes with as-yet-uncharacterized knockout phenotypes (such as *Rorα* or *E4bp4*) are shown to be essential, a similar approach will allow us to identify the regulatory interactions underlying their essentiality.

Experimental predictions

Ensemble-based parameterization allows us to quantify uncertainty in our predictions of experimental results. Because

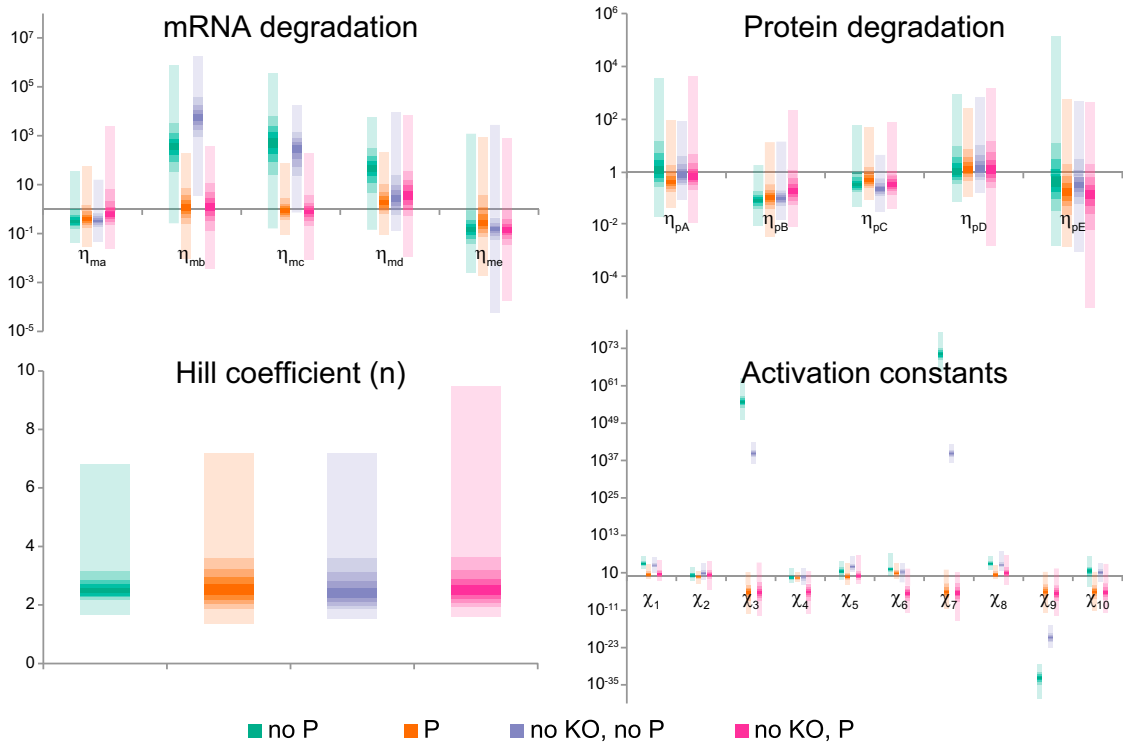

FIGURE 4 Parameter distributions for the four different scoring scenarios; data series are named as in Fig. 3. The probability constraint term suppresses overly fast mRNA turnover and keeps activation constants confined within a narrow range but has little effect on protein degradation rates or the Hill coefficient. To see this figure in color, go online.

the model was parameterized with system-level data, it will be most useful to make a prediction of system-level behavior, determining how the clock as a complete system will respond to a perturbation.

PRCs are used in chronobiology to describe the effect of external signals (light, chemicals, etc.) on the phase of the clock (42). A PRC is obtained by plotting the phase shift as a function of the preperturbation phase. For example, under constant-dark conditions, an early-morning light pulse will shift the clock to an earlier time (dawn is perceived to have come early), whereas an evening pulse produces a positive phase shift (dusk is perceived to have come late). Under constant-light conditions, a dark-pulse PRC can also be constructed by briefly turning the lights off at defined times.

Although our model does not explicitly incorporate the effects of external stimuli, phase-response curves can be calculated for differential perturbations to the state variables. In cultured SCN slices, phase shifts have been observed as a result of chemical stimulation (43–46), but the connection between the signal-response cascades and the core clockwork is unclear, especially for the dark-pulse response. For example, external stimulation could lead to transcription activation, targeted protein degradation, or other downstream effects. If the phase response of state variable perturbations is similar to that of experimental perturbations, one can begin to search for a causal link between external perturbations and internal changes.

Fig. 5 shows the PRCs calculated for perturbations to the five mRNA components of the model (see Fig. S6 for protein components). The PRCs calculated for the parameterizations with and without the probability constraints have similar shapes, but sometimes wildly different magnitudes. The shape of the PRC curves can be compared with "light-type" PRCs such as N-Methyl-D-aspartate (NMDA) (47) or "dark-type" PRCs such as NPY (48). Such comparisons should be made cautiously, however; the experimental data come from organotypic slice cultures in the case of NMDA or intact mice in the case of NPY and may reflect higher-level effects that are not observed in the single-cell clock.

The PRCs for *Dbp* and *RevErbα* show some similarities to NMDA. Light stimulation has been known to promote *Per1/2* transcription (49–51); all four of these genes have expression schedules that are controlled by an E/E'-box. Stronger similarities can be seen between the dark-type PRC for NPY and the calculated PRC for *Cry1*. The mechanism by which NPY affects the core clockwork is still unclear; *Cry1* may be a fruitful target for future investigation.

The NMDA data of Asai et al. (47) used cultured SCN slices for which circadian time is more difficult to interpret than in an intact rodent. They defined CT0 as the luminescence peak of luciferase driven by a *Per1* promoter. When SCN tissues are synchronized to an external zeitgeber, the luminescence peak coincides with the middle of the light period (52). All of our experimental protein/mRNA phases (as well as the

NPY PRC) were drawn from intact rodents subjected to a light period lasting from CT0-12. The luminescence peak should be at roughly CT6; the data points in Fig. 5 are shifted by 6 h relative to the presentation in Asai et al.

The PRC for *E4bp4* is more enigmatic. In the probability-constrained calculation, perturbations to *E4bp4* levels have virtually no effect on the phase. When the model is optimized without probability constraints, the effects of perturbations to *E4bp4* levels are huge. As was mentioned above, Fig. 4 suggests that *E4bp4* may be a circadian output, rather than an integral part of the core feedback loops. In this case, we would expect direct perturbations to have no effect on the core clockwork.

The PRC shapes can be interpreted using Fig. 2, which shows mRNA concentrations as a function of circadian time. The expression level of *Cry1* peaks around lights-off (CT12) and has a minimum near lights-on (CT0); the extrema for CRY1 protein will be about 2 h later. If *Cry1* levels are increased during the daytime, when its levels are rising, the clock will speed up as shown by the positive daytime amplitude in Fig. 5. Conversely, an increase in *Cry1* during the night will prolong its decline and slow down the clock, consistent with the negative nighttime amplitude. In general, PRCs cross the x axis in the negative direction near the abundance peak, and they cross in the positive direction near the abundance minimum.

A related test of our model's predictive power is suggested by the rescue of $Cry1^{-/-}$:$Cry2^{-/-}$ knockout cells using exogenous *Cry1* driven by a synthetic promoter (18). When the phase of *Cry1* expression was altered by using synthetic promoters with varying numbers of D-box and RRE elements, it was found that weakening of the D-box regulation correlates with a later peak of CRY1 expression (relative to the period) and an overall lengthening of the circadian period. We can mimic this effect by rescaling χ_4 and χ_7, which control the binding of DBP and E4BP4 to the promoter region of *Cry1*. For the optimized parameter set, a decrease in these two binding constants led to a diminished role for the D-box in the regulation of *Cry1*, leading in turn to a phase delay of CRY1 expression and an increase in the oscillation period (Fig. 6), consistent with the experimental trend.

When eight parameter sets were randomly chosen from the MMC ensemble, seven show the expected positive trend. Period/phase curves were calculated for modified versions of 6400 MC-sampled parameter sets. The resulting distribution of points is mostly in the positive quadrant (lengthened period and delayed CRY1 phase), suggesting an overall trend that agrees qualitatively with experiments. It may be possible to generalize: systems-level outputs become less consistent as they are less similar to the type of behavior used to parameterize the model. Our score

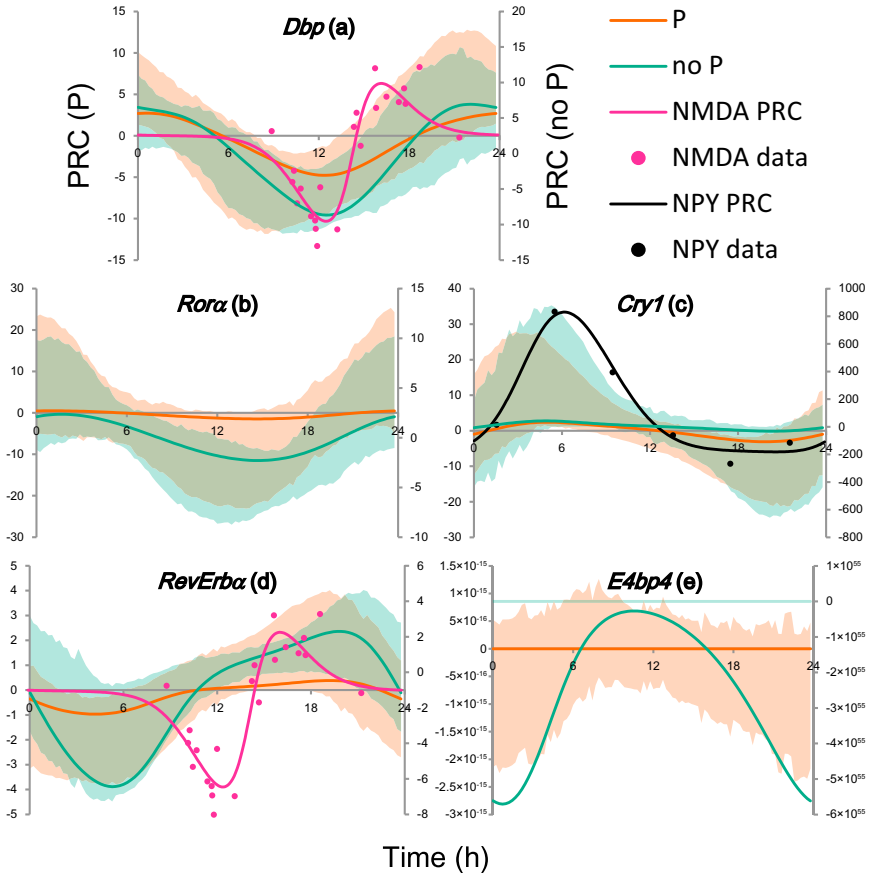

FIGURE 5 Phase response curves for the five mRNA components in the model. PRCs were calculated both with ("P") and without ("no P") probability constraints, and shaded regions contain 80% of the curves from a Monte Carlo ensemble. The left y axis shows the scale for the "P" ensemble; the right axis shows the scale for the "no P" ensemble. The calculated PRC for an increase in *Cry1* expression is qualitatively similar to a measured PRC for neuropeptide Y (NPY), whereas the calculated PRCs for *Dbp* and *RevErbα* share some features in common with the PRC for NMDA. Similar plots for the protein components can be found in Fig. S6. To see this figure in color, go online.

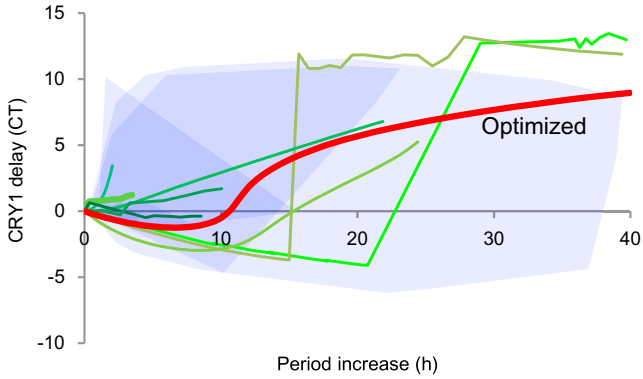

FIGURE 6 Effects of weakening the D-box regulation of *Cry1* The *x* axis indicates the increase in period length (beyond the original ~24 h), and the *y* axis shows the increase in the CRY1 phase (from the original CT 14), normalized to circadian time. For the parameter set optimized with probability constraints, weaker D-box regulation results in a longer oscillation period and a later CRY1 peak (relative to the period length). When eight random samples were drawn from a Monte Carlo ensemble, the same positive trend was observed in seven of them. Shaded regions show convex hulls containing the period/delay curves for parameters drawn from the MC ensemble; the outermost hull contains 90% of points. To see this figure in color, go online.

function largely measured the shape of the limit cycle. The abundance oscillations shown in Fig. 2 show behavior on the limit cycle and are quite consistent. PRCs (Fig. 5) show the effects of small perturbations from the limit cycle and are still fairly consistent. The *Cry1/2* rescue experiments perturb the system significantly from the wild-type limit cycle, and only qualitative predictions can be made with any confidence.

Cleaning up sloppy models

Model sloppiness poses a challenge for systems biology—if a model is parameterized to systems-level data, estimates for the values of individual parameters are often unreliable. Because the physical environment of the cell differs from the dilute solutions used in most in vitro assays, experimental estimates of parameter values will often be of limited utility. Furthermore, whereas the "sloppy" eigendirections are severely underconstrained by systems-level data, the "stiff" eigendirections are often more tightly constrained than they would be by direct experimental measurement (3). A model built with directly measured parameters will often be less able to reproduce systems-level data than a sloppy model parameterized at the systems level.

This is not to say that individual parameter values are irrelevant to systems-level predictions. For example, because concentration scales are arbitrary in our dimensionless model, mRNA or protein degradation rates can increase significantly, as long as they are offset by increases in the χ parameters that control the protein's ability to regulate other genes. Phase response calculations, however, require taking a derivative of the phase with respect to a perturbation to a concentration variable—the absolute value of these dimensionless variables determines the scale of the PRC. The extreme variability of the χ parameters related to *E4bp4* (χ_3 and χ_7 as inputs, χ_9 and χ_{10} as inputs; see Fig. 4) is therefore reflected in the wildly differing scales of *E4bp4* PRCs in Fig. 5.

Our solution to this problem is facilitated by recent genome-scale surveys of the synthesis and degradation rates of proteins and mRNAs. Even if the components of a model cannot be identified with any of the measured species, large data sets can be used to construct previous probability distributions for model parameters. Fig. 2 indicates that the presence of probability constraints results in only minor changes to the model outputs, whereas Figs. 3 and 4 show dramatic decreases in parameter variability.

Knockout predictions

Our simplified model eliminates much of the redundancy of the real clock system and is less resilient to gene knockouts than the actual system. Knockouts of *Cry1/2* are arrhythmic because of the network topology (29); if C is removed from the diagram in Fig. 1 *C*, no closed negative feedback loops persist. The *Rev-Erbα* knockout is required to be arrhythmic by our scoring scheme (15), although many parameter sets showed damped oscillations to a stable fixed point. Other possible knockouts have not been as well-characterized experimentally and are discussed below and in Table 2.

Dbp/Tef/Hlf

If these D-box activators are knocked out, *Rorα* also will not be synthesized; because *A* and *B* are activators required for the transcription of *Cry1*, this precludes oscillations. The concentrations of *Rorα/β*, *Cry1*, and *E4bp4* should decrease dramatically. If this mutation does not affect these levels at all (particularly *Rorα/β*, which contain D-boxes), then the

TABLE 2 Effects of modeled knockout mutations

Mutant	Predicted rhythmicity	Predicted expression changes	Experimental observation	Reference(s)
Dbp/Tef/Hlf	Arrhythmic due to model topology	*Ror*, *Cry1*, *E4bp4* all decrease dramatically	Rhythmic	(27)
Rorα/β	Damped oscillations	*E4bp4* decreases	Rhythmic?	(54,55)
Cry1/2	Arrhythmic due to model topology	*Dbp/Tef/Hlf*, *Ror*, *RevErb*, *E4bp4* all increase	Arrhythmic	(29)
RevErbα/β	Arrhythmic due to constraint; sometimes shows damped oscillations	*Dbp/Tef/Hlf* decreases; others do not change much	Arrhythmic	(15)
E4bp4	Rhythmic	No effect		

system may contain an additional D-box activator (either oscillatory or constitutive) that is compensating for the loss of *Dbp/Tef/Hlf*. If instead, *Rorα/β* levels do decrease and the phenotype is similar to the removal of D-box regulation from *Cry1* (Fig. 6) with a later *Cry1* phase and a longer period, this suggests that D-box mediated expression is affected but RRE-mediated expression is not. In such a case, it is possible that the RRE is being activated by a pathway other than the D-box-mediated ROR proteins.

Rorα/β

Knocking out the *Ror* genes does not abolish *Cry1* (which is also activated by DBP/TEF/HLF), but it does abolish *E4bp4*. The remaining three genes do not form any closed feedback loops, so sustained oscillations are impossible. Members of the MMC ensemble with probability and knockout constraints generally show damped oscillations; in ~ 30% of cases this damping is fairly slow (i.e., more than a few oscillation periods are observed) and population-level oscillations may still be possible, similar to *Per1* and *Cry1* single-knockout mutants (53). Levels of *E4bp4* decrease dramatically, but changes to *Cry1* are smaller. This is probably because the *Ror* genes have incoherent effects on *Cry1*, both activating it directly and repressing it indirectly via *E4bp4*. If arrhythmicity and a decrease in *E4bp4* are not observed, then RRE expression may be activated by a different pathway. Experimentally, the *Rorα* knockout shows a shortened circadian period (54), whereas the *Rorβ* knockout shows a lengthened one (55); the double-knockout has (to our knowledge) not yet been characterized.

E4bp4

When parameter sets are drawn from the MMC ensemble with probability and knockout constraints, simulated knockouts of *E4bp4* have no effect on the period, the fit quality, or the correctness of other knockout phenotypes (*RevErbα*, *Cry1*ΔD, *Cry1*ΔRRE). This is consistent with our interpretation of Figs. 4 and 5—*E4bp4* may function primarily as an output gene, rather than a core component of the clock.

DISCUSSION

A new view of the mammalian clock

Models that focus on the central *Per-Cry/Bmal1-Clock* feedback loop have been successful at reproducing several aspects of the circadian clock, such as gene knockout phenotypes (10,12–14) and entrainment to light stimuli (10,11). The recent finding that *Cry1* is best regarded as being co-regulated by the RRE and the D-box (rather than the E/E'-box) will require a different topological organization for future models. Although our model is less detailed than many in the literature, it more correctly describes the transcriptional regulation of *Cry1* (18). Our decision not to include *Per1* and *Per2* in the model was motivated primarily by the current incomplete state of knowledge about the detailed biochemical mechanisms of these two important components, in particular the unusually long delay between their mRNA and protein expression peaks (22,35,36). As more reliable experimental characterizations of these genes and their products become available, it will be possible to incorporate them into our modeling framework.

Our results suggest that the current understanding of the D-box and its role is far from complete. When the model is optimized with parameter constraints, the parameters governing the effects of E4BP4 (a D-box repressor) on *Cry1* and *Rorα* take on extremely low values (Fig. 4), suggesting that the observed expression patterns for these genes can be fit without any significant help from *E4bp4*. The inconsistent, extremely low-amplitude PRC for *E4bp4* (Fig. 5) likewise indicates that *E4bp4* may function primarily as a circadian output, rather than as a central part of the clockwork.

At the same time, experiments show that (at least in cultured cells) D-box regulation is essential for the correct timing of *Cry1* expression (18). It is possible that the effects of the D-box on the core clockwork are mediated solely by the D-box activators *Dbp/Tef/Hlf* or that the essentiality of *E4bp4* depends on interactions that were not included in our model. In any case, careful experimental studies of D-box-binding transcription factors and their targets are likely to yield valuable insights into clock function.

Experimental perturbations

PRCs are determined experimentally by perturbing the clock system using a stimulus—light, neurotransmitters, etc.—that has an indirect effect on the core clock system, mediated by signaling pathways. A more direct (and possibly feasible) approach would be transient overexpression of a clock gene in cultured cells. Simple genetic circuits such as an incoherent feed-forward loop can generate transient pulses of gene expression in response to an external signal (56,57). If an exogenous clock gene driven by this type of circuit were transfected into a cell line containing a bioluminescent circadian reporter, one could observe the effects of an overexpression pulse on the clock's phase. This type of protocol avoids the problems of redundancy. For example, our model gene *b* (a D-box driven activator of the RRE) could correspond to *Rorα* or *Rorβ*, and other redundant genes may yet be discovered. Overexpression of a single redundant gene, however, may be sufficient to produce the expected phase shift. This contrasts with knockout experiments in which all redundant versions of a gene must be removed before an effect is observed.

Mechanism of chemically induced phase resetting

Previous models of the mammalian clock have focused on the light-stimulated induction of *Per1/2* transcription as

the sole external input to the clock (10,11,58,59). Although this is undoubtedly important, it is likely that other pathways exist, particularly for nonphotic signals such as NPY. Because it focuses on a different feedback loop structure than what has traditionally been employed in clock models, our model provides an ideal tool with which to search for other possible modes of perturbation.

Comparison of our calculated PRCs with experimentally derived PRCs (Fig. 5), suggests that photic signals such as NMDA may act by stimulating the synthesis of E/E'-box controlled genes such as *Dbp* or *RevErbα*, consistent with the light stimulation of E/E'-box-regulated *Per*. In addition, nonphotic signals such as NPY may act on the core clockwork by increasing the expression of *Cry1*.

SUPPORTING MATERIAL

Six figures, two tables, and supporting text are available at http://www.biophysj.org/biophysj/supplemental/S0006-3495(14)00740-1

C. C. J. and D. P. are supported by the RIKEN Foreign Postdoctoral Researcher Program. Calculations used the RIKEN Integrated Cluster of Clusters. This research was supported by an intramural Grant-in-Aid from the RIKEN Center for Developmental Biology and the Quantitative Biology Center (H. R. U.), the Uehara Memorial Foundation (H. R. U.), the Mitsubishi Foundation (H. R. U.), the President's Fund from RIKEN (H. R. U.), and a Grant-in-Aid for Scientific Research on Innovative Areas (No. 3306) from the Ministry of Education, Culture, Sports, Science, and Technology, Japan (H. R. U.).

The authors would also like to thank Rikuhiro Yamada for helpful discussions.

REFERENCES

1. Dyson, F. 2004. A meeting with Enrico Fermi. *Nature.* 427:297–298.
2. Brown, K. S., and J. P. Sethna. 2003. Statistical mechanical approaches to models with many poorly known parameters. *Phys. Rev. E Stat. Nonlin. Soft Matter Phys.* 68:021904.
3. Gutenkunst, R. N., J. J. Waterfall, …, J. P. Sethna. 2007. Universally sloppy parameter sensitivities in systems biology models. *PLOS Comput. Biol.* 3:1871–1878.
4. Daniels, B. C., Y. J. Chen, …, C. R. Myers. 2008. Sloppiness, robustness, and evolvability in systems biology. *Curr. Opin. Biotechnol.* 19:389–395.
5. Raue, A., C. Kreutz, …, J. Timmer. 2009. Structural and practical identifiability analysis of partially observed dynamical models by exploiting the profile likelihood. *Bioinformatics.* 25:1923–1929.
6. Press, W. H. 2007. Numerical Recipes: The Art of Scientific Computing. Cambridge University Press, New York.
7. Joshi, M., A. Seidel-Morgenstern, and A. Kremling. 2006. Exploiting the bootstrap method for quantifying parameter confidence intervals in dynamical systems. *Metab. Eng.* 8:447–455.
8. St John, P. C., and F. J. Doyle, 3rd. 2013. Estimating confidence intervals in predicted responses for oscillatory biological models. *BMC Syst. Biol.* 7:71.
9. Metropolis, N., and S. Ulam. 1949. The Monte Carlo method. *J. Am. Stat. Assoc.* 44:335–341.
10. Forger, D. B., and C. S. Peskin. 2003. A detailed predictive model of the mammalian circadian clock. *Proc. Natl. Acad. Sci. USA.* 100:14806–14811.
11. Leloup, J. C., and A. Goldbeter. 2003. Toward a detailed computational model for the mammalian circadian clock. *Proc. Natl. Acad. Sci. USA.* 100:7051–7056.
12. Becker-Weimann, S., J. Wolf, …, A. Kramer. 2004. Modeling feedback loops of the mammalian circadian oscillator. *Biophys. J.* 87:3023–3034.
13. Mirsky, H. P., A. C. Liu, …, F. J. Doyle, 3rd. 2009. A model of the cell-autonomous mammalian circadian clock. *Proc. Natl. Acad. Sci. USA.* 106:11107–11112.
14. Kim, J. K., and D. B. Forger. 2012. A mechanism for robust circadian timekeeping via stoichiometric balance. *Mol. Syst. Biol.* 8:630.
15. Cho, H., X. Zhao, …, R. M. Evans. 2012. Regulation of circadian behaviour and metabolism by REV-ERB-α and REV-ERB-β. *Nature.* 485:123–127.
16. Hogenesch, J. B., and H. R. Ueda. 2011. Understanding systems-level properties: timely stories from the study of clocks. *Nat. Rev. Genet.* 12:407–416.
17. Ukai-Tadenuma, M., T. Kasukawa, and H. R. Ueda. 2008. Proof-by-synthesis of the transcriptional logic of mammalian circadian clocks. *Nat. Cell Biol.* 10:1154–1163.
18. Ukai-Tadenuma, M., R. G. Yamada, …, H. R. Ueda. 2011. Delay in feedback repression by cryptochrome 1 is required for circadian clock function. *Cell.* 144:268–281.
19. Hogenesch, J. B., W. K. Chan, …, C. A. Bradfield. 1997. Characterization of a subset of the basic-helix-loop-helix-PAS superfamily that interacts with components of the dioxin signaling pathway. *J. Biol. Chem.* 272:8581–8593.
20. Gekakis, N., D. Staknis, …, C. J. Weitz. 1998. Role of the CLOCK protein in the mammalian circadian mechanism. *Science.* 280:1564–1569.
21. Ueda, H. R., S. Hayashi, …, S. Hashimoto. 2005. System-level identification of transcriptional circuits underlying mammalian circadian clocks. *Nat. Genet.* 37:187–192.
22. Yoo, S. H., C. H. Ko, …, J. S. Takahashi. 2005. A noncanonical E-box enhancer drives mouse Period2 circadian oscillations in vivo. *Proc. Natl. Acad. Sci. USA.* 102:2608–2613.
23. Falvey, E., L. Marcacci, and U. Schibler. 1996. DNA-binding specificity of PAR and C/EBP leucine zipper proteins: a single amino acid substitution in the C/EBP DNA-binding domain confers PAR-like specificity to C/EBP. *Biol. Chem.* 377:797–809.
24. Harding, H. P., and M. A. Lazar. 1993. The orphan receptor Rev-ErbA alpha activates transcription via a novel response element. *Mol. Cell. Biol.* 13:3113–3121.
25. Preitner, N., F. Damiola, …, U. Schibler. 2002. The orphan nuclear receptor REV-ERBalpha controls circadian transcription within the positive limb of the mammalian circadian oscillator. *Cell.* 110:251–260.
26. Ueda, H. R., W. Chen, …, S. Hashimoto. 2002. A transcription factor response element for gene expression during circadian night. *Nature.* 418:534–539.
27. Gachon, F., P. Fonjallaz, …, U. Schibler. 2004. The loss of circadian PAR bZip transcription factors results in epilepsy. *Genes Dev.* 18:1397–1412.
28. Storn, R., and K. Price. 1997. Differential evolution—a simple and efficient heuristic for global optimization over continuous spaces. *J. Glob. Optim.* 11:341–359.
29. van der Horst, G. T., M. Muijtjens, …, A. Yasui. 1999. Mammalian Cry1 and Cry2 are essential for maintenance of circadian rhythms. *Nature.* 398:627–630.
30. Sharova, L. V., A. A. Sharov, …, M. S. Ko. 2009. Database for mRNA half-life of 19 977 genes obtained by DNA microarray analysis of pluripotent and differentiating mouse embryonic stem cells. *DNA Res.* 16:45–58.
31. Schwanhäusser, B., D. Busse, …, M. Selbach. 2011. Global quantification of mammalian gene expression control. *Nature.* 473:337–342.
32. Nalefski, E. A., E. Nebelitsky, …, S. R. Gullans. 2006. Single-molecule detection of transcription factor binding to DNA in real time: specificity, equilibrium, and kinetic parameters. *Biochemistry.* 45:13794–13806.

33. Kolesov, G., Z. Wunderlich, …, L. A. Mirny. 2007. How gene order is influenced by the biophysics of transcription regulation. *Proc. Natl. Acad. Sci. USA.* 104:13948–13953.

34. Strogatz, S. H. 1994. Nonlinear Dynamics and Chaos: With Applications to Physics, Biology, Chemistry, and Engineering. Addison-Wesley, Reading, MA.

35. Debruyne, J. P., E. Noton, …, S. M. Reppert. 2006. A clock shock: mouse CLOCK is not required for circadian oscillator function. *Neuron.* 50:465–477.

36. Lee, C., J. P. Etchegaray, …, S. M. Reppert. 2001. Posttranslational mechanisms regulate the mammalian circadian clock. *Cell.* 107: 855–867.

37. Mitsui, S., S. Yamaguchi, …, H. Okamura. 2001. Antagonistic role of E4BP4 and PAR proteins in the circadian oscillatory mechanism. *Genes Dev.* 15:995–1006.

38. Stratmann, M., F. Stadler, …, J. A. Ripperger. 2010. Flexible phase adjustment of circadian albumin D site-binding protein (DBP) gene expression by CRYPTOCHROME1. *Genes Dev.* 24:1317–1328.

39. Schneider, C. A., W. S. Rasband, and K. W. Eliceiri. 2012. NIH Image to ImageJ: 25 years of image analysis. *Nat. Methods.* 9:671–675.

40. Nelder, J. A., and R. Mead. 1965. A simplex-method for function minimization. *Comput. J.* 7:308–313.

41. Kramer, M. A., H. Rabitz, and J. M. Calo. 1984. Sensitivity analysis of oscillatory systems. *Appl. Math. Model.* 8:328–340.

42. Dunlap, J. C., J. J. Loros, and P. J. DeCoursey. 2004. Chronobiology: Biological Timekeeping. Sinauer Associates, Sunderland, MA.

43. Prosser, R. A., R. R. Dean, …, J. D. Miller. 1993. Serotonin and the mammalian circadian system: I. In vitro phase shifts by serotonergic agonists and antagonists. *J. Biol. Rhythms.* 8:1–16.

44. Hamada, T., S. Shibata, …, S. Watanabe. 1993. Effect of somatostatin on circadian rhythms of firing and 2-deoxyglucose uptake in rat suprachiasmatic slices. *Am. J. Physiol.* 265:R1199–R1204.

45. Trachsel, L., H. C. Heller, and J. D. Miller. 1995. Nicotine phase-advances the circadian neuronal activity rhythm in rat suprachiasmatic nuclei explants. *Neuroscience.* 65:797–803.

46. Biello, S. M., D. A. Golombek, and M. E. Harrington. 1997. Neuropeptide Y and glutamate block each other's phase shifts in the suprachiasmatic nucleus in vitro. *Neuroscience.* 77:1049–1057.

47. Asai, M., S. Yamaguchi, …, H. Okamura. 2001. Visualization of mPer1 transcription in vitro: NMDA induces a rapid phase shift of mPer1 gene in cultured SCN. *Curr. Biol.* 11:1524–1527.

48. Huhman, K. L., and H. E. Albers. 1994. Neuropeptide Y microinjected into the suprachiasmatic region phase shifts circadian rhythms in constant darkness. *Peptides.* 15:1475–1478.

49. Albrecht, U., Z. S. Sun, …, C. C. Lee. 1997. A differential response of two putative mammalian circadian regulators, mper1 and mper2, to light. *Cell.* 91:1055–1064.

50. Shearman, L. P., M. J. Zylka, …, S. M. Reppert. 1997. Two period homologs: circadian expression and photic regulation in the suprachiasmatic nuclei. *Neuron.* 19:1261–1269.

51. Shigeyoshi, Y., K. Taguchi, …, H. Okamura. 1997. Light-induced resetting of a mammalian circadian clock is associated with rapid induction of the mPer1 transcript. *Cell.* 91:1043–1053.

52. Inagaki, N., S. Honma, …, K. Honma. 2007. Separate oscillating cell groups in mouse suprachiasmatic nucleus couple photoperiodically to the onset and end of daily activity. *Proc. Natl. Acad. Sci. USA.* 104:7664–7669.

53. Liu, A. C., D. K. Welsh, …, S. A. Kay. 2007. Intercellular coupling confers robustness against mutations in the SCN circadian clock network. *Cell.* 129:605–616.

54. Sato, T. K., S. Panda, …, J. B. Hogenesch. 2004. A functional genomics strategy reveals Rora as a component of the mammalian circadian clock. *Neuron.* 43:527–537.

55. André, E., F. Conquet, …, M. Becker-André. 1998. Disruption of retinoid-related orphan receptor beta changes circadian behavior, causes retinal degeneration and leads to vacillans phenotype in mice. *EMBO J.* 17:3867–3877.

56. Mangan, S., and U. Alon. 2003. Structure and function of the feed-forward loop network motif. *Proc. Natl. Acad. Sci. USA.* 100:11980–11985.

57. Basu, S., R. Mehreja, …, R. Weiss. 2004. Spatiotemporal control of gene expression with pulse-generating networks. *Proc. Natl. Acad. Sci. USA.* 101:6355–6360.

58. Okamura, H., S. Miyake, …, G. T. J. van der Horst. 1999. Photic induction of mPer1 and mPer2 in cry-deficient mice lacking a biological clock. *Science.* 286:2531–2534.

59. Zylka, M. J., L. P. Shearman, …, S. M. Reppert. 1998. Three period homologs in mammals: differential light responses in the suprachiasmatic circadian clock and oscillating transcripts outside of brain. *Neuron.* 20:1103–1110.